

Antitumor and Antiangiogenic Properties of Gold(III) Complexes Containing Cycloaurated Triphenylphosphine Sulfide Ligands

T. Srinivasa Reddy, Steven H. Privér, Nedaossadat Mirzadeh,* Rodney B. Luwor, Velma Ganga Reddy, Shwathy Ramesan, and Suresh K. Bhargava*

Cite This: <https://dx.doi.org/10.1021/acs.inorgchem.0c00423>

Read Online

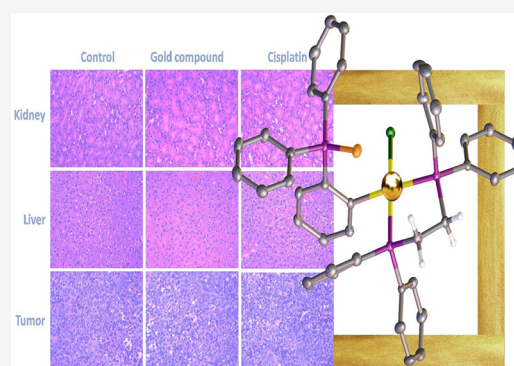
ACCESS |

Metrics & More

Article Recommendations

Supporting Information

ABSTRACT: A family of stable anticancer gold(III)-based therapeutic complexes containing cyclometalated triphenylphosphine sulfide ligands have been prepared. The anticancer properties of the newly developed complexes $[\text{AuCl}_2\{\kappa^2\text{-}2\text{-C}_6\text{H}_4\text{P}(\text{S})\text{Ph}_2\}]$ (1), $[\text{Au}(\kappa^2\text{-S}_2\text{CNEt}_2)\{\kappa^2\text{-}2\text{-C}_6\text{H}_4\text{P}(\text{S})\text{Ph}_2\}]\text{PF}_6$ (2), $[\text{AuCl}(\text{dppe})\{\kappa\text{-}2\text{-C}_6\text{H}_4\text{P}(\text{S})\text{Ph}_2\}]\text{Cl}$ (3), and $[\text{Au}(\text{dppe})\{\kappa^2\text{-}2\text{-C}_6\text{H}_4\text{P}(\text{S})\text{Ph}_2\}]\text{PF}_6$ (4) were investigated toward five human cancer cell lines [cervical (HeLa), lung (A549), prostate (PC3), fibrosarcoma (HT1080), and breast (MDA-MB-231)]. *In vitro* cytotoxicity studies revealed that compounds 2–4 displayed potent cell growth inhibition (IC_{50} values in the range of 0.17–2.50 μM), comparable to, or better than, clinically used cisplatin (0.63–6.35 μM). Preliminary mechanistic studies using HeLa cells indicate that the cytotoxic effects of the compounds involve apoptosis induction through ROS accumulation. Compound 2 also demonstrated significant inhibition of endothelial cell migration and tube formation in the angiogenesis process. Evaluation of the *in vivo* antitumor activity of compound 2 in nude mice bearing cervical cancer cell (HeLa) xenografts indicated significant tumor growth inhibition (55%) with 1 mg/kg dose (every 3 days) compared with the same dose of cisplatin (28%). These results demonstrate the potential of gold(III) complexes containing cyclometalated triphenylphosphine sulfide ligands as novel metal-based anticancer agents.



INTRODUCTION

In response to the adverse side effects of the clinically approved anticancer drug cisplatin, gold complexes have been investigated with the aim of delivering metal-based therapeutics with minimal side effects.^{1–4} The promising outlook of gold-based therapeutics lies in their ability to present effective anticancer properties with high selectivity toward cancer cells, however their poor stability toward reduction under physiological conditions must be addressed in order to advance their clinical translation. Gold(III) complexes are particularly prone to reduction, therefore their potential in the development of therapeutic agents has been explored to a lesser extent compared to their gold(I) rivals.^{1–5} Despite these limitations, mechanistic studies on several gold(III) complexes have been recently reported.⁶

The inclusion of a cyclometalated ring for the structural modification of gold(III) complexes has been proposed recently as a strategy to enhance their stability under physiological conditions, minimizing undesired intracellular redox reactions as a result of the strength of the gold–carbon σ -bond in the cyclometalated moiety.¹ This strategy has been applied to the preparation of cycloaurated gold(III) complexes containing C–N, C–N–C, and C–N–N ligands shown in Figure 1.^{1,2}

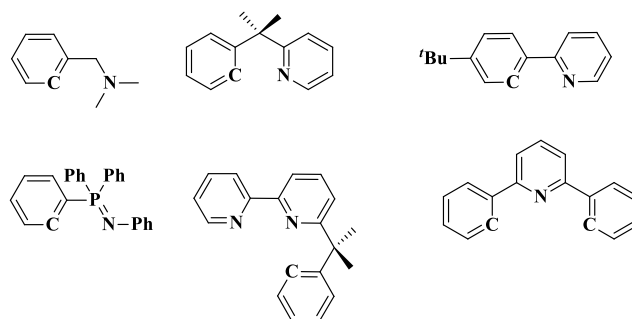


Figure 1. Bidentate C–N and tridentate C–N–C and C–N–N ligands used in the development of cycloaurated anticancer gold(III) complexes.

Received: February 10, 2020

Among these ligands, the iminophosphorane compound has enabled the development of a unique class of gold(III) complexes, shown in Figure 2, whose stability in solution can be easily monitored by ^{31}P NMR spectroscopy. Complexes A and B exhibit high *in vitro* stability in DMSO, whereas C is only stable for 24 h. In all cases, these gold(III) compounds showed high toxicity against Jurkat T-cell acute lymphoblastic leukemia cells and B-CLL cells.^{7,8}

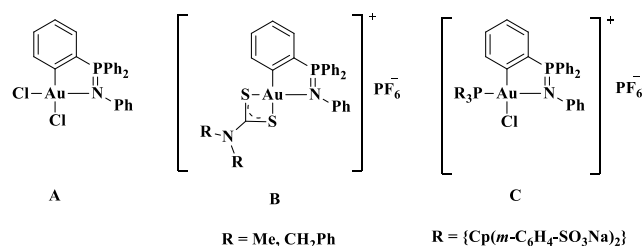


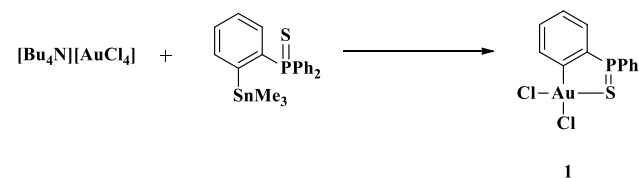
Figure 2. Examples of cycloaurated gold(III) complexes containing an iminophosphorane ligand.

In alignment with our current research in developing gold complexes for the treatment of cancer^{8–16} and inspired by the potential of iminophosphorane ligands in the medicinal chemistry field, we have designed and extended a class of cycloaurated gold(III) complexes derived from triphenylphosphine sulfide (Figure 3). In contrast to our previously published work on ionic digold(I/III) complexes containing two cyclometalated triphenylphosphine sulfide ligands,¹⁶ the results herein are for a series of mononuclear gold(III) complexes containing only one cyclometalated ligand. The anticancer properties and mechanism of action of the gold(III) complexes 1–4 containing a cycloaurated C–S moiety were investigated toward a wide range of cancer cell lines, the results of which are presented here.

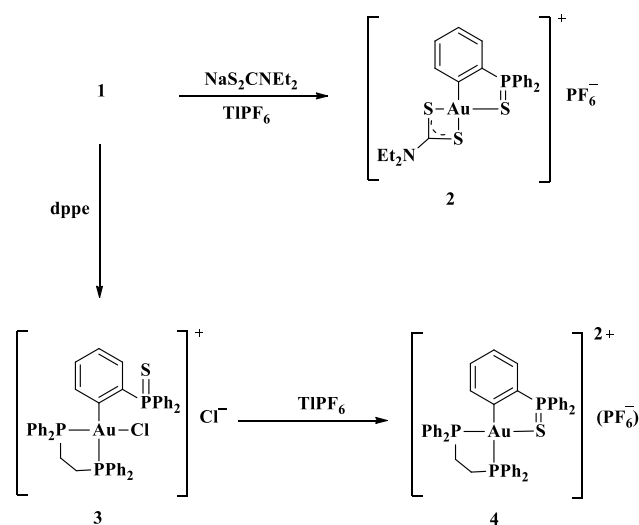
RESULTS AND DISCUSSIONS

Synthesis of Gold Complexes. The reaction of $[\text{Bu}_4\text{N}][\text{AuCl}_4]$ with an equimolar amount of $2\text{-Me}_3\text{SnC}_6\text{H}_4\text{P}(\text{S})\text{Ph}_2$ in dichloromethane led to the formation of $[\text{AuCl}_2\{\kappa^2\text{-}2\text{-C}_6\text{H}_4\text{P}(\text{S})\text{Ph}_2\}]$ (**1**; Scheme 1) as a pale yellow solid in 94%. This compound has been prepared previously in 42–46% yield by the transmetalation of the organomercurials $[\text{HgCl}\{\kappa\text{-C-C}_6\text{H}_4\text{P}(\text{S})\text{Ph}_2\}_2]$ or $[\text{Me}_4\text{N}][\text{AuCl}_4]$ in acetonitrile.¹⁷ Treatment of **1** with $\text{NaS}_2\text{CNEt}_2$ or 1,2-bis(diphenylphosphino)ethane (dppe) afforded $[\text{Au}(\kappa^2\text{-S}_2\text{CNEt}_2)\{\kappa^2\text{-}2\text{-C}_6\text{H}_4\text{P}(\text{S})\text{Ph}_2\}]\text{PF}_6$ (**2**) and $[\text{AuCl}(\text{dppe})\{\kappa^2\text{-}2\text{-C}_6\text{H}_4\text{P}(\text{S})\text{Ph}_2\}]\text{Cl}$ (**3**), respectively (Scheme 2). In the presence of TIPF_6 , **1** reacted with dppe to give $[\text{Au}(\text{dppe})\{\kappa^2\text{-}2\text{-C}_6\text{H}_4\text{P}(\text{S})\text{Ph}_2\}][\text{PF}_6]_2$ (**4**). Complexes 1–4 were charac-

Scheme 1. Synthesis of $[\text{AuCl}_2\{\kappa^2\text{-}2\text{-C}_6\text{H}_4\text{P}(\text{S})\text{Ph}_2\}]$ (**1**)



Scheme 2. Synthesis of the Cationic Gold(III) Complexes 2–4



terized by multinuclear NMR spectroscopy and, in the case of complexes **1**, **3**, and **4**, by single crystal X-ray diffraction.

The ^1H NMR spectra for complexes 1–4 all showed the expected aromatic multiplets in the range δ 7.3–7.9. In addition, the spectrum for complex **2** showed two broad multiplet resonances at δ 1.29 and 3.83 due to the methyl and methylene protons of the dithiocarbamate ligand, respectively. For complexes **3** and **4**, the methylene protons of the dppe ligand appeared as two broad multiplets between δ 3 and 4. The ^{31}P NMR spectra for complexes **1** and **2** showed a singlet resonance at δ 56.1 and 61.1, respectively, the chemical shift of which is typical of coordinated tertiary phosphine sulfide^{16,17} and similar to that of the cycloiminophosphorane complex $[\text{AuCl}_2\{\kappa^2\text{-}2\text{-C}_6\text{H}_4\text{P}(\text{NPh})\text{Ph}_2\}]$ (δ 65).¹⁸ The ^{31}P NMR spectra of **3** and **4** were more complex and showed three resonances in a 1:1:1 ratio in the region δ 45–77, assignable to the phosphorus nuclei in the dppe ligand and $\text{C}_6\text{H}_4\text{P}(\text{S})\text{Ph}_2$ group. Although the exact assignment of each resonance was not possible, the resonances show fine structure due to P–P

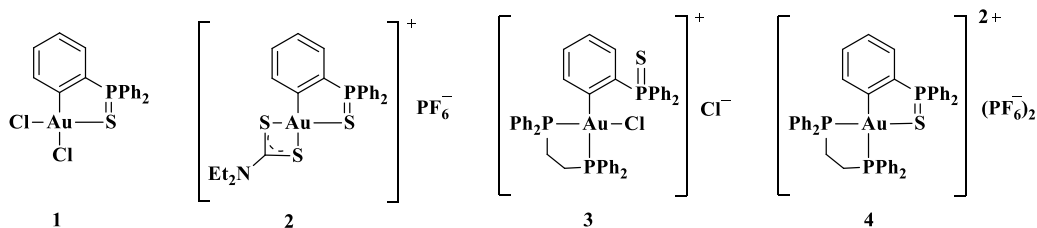


Figure 3. Cycloaurated gold(III) complexes derived from triphenylphosphine sulfide.

coupling. The spectra of **2** and **4** also showed the expected septet at $\delta -144$ due to the PF_6^- anion.

The structures of **1**, **3** (shown in Figure 4), and **4** (shown in Figure 5) were confirmed by X-ray diffraction. In all cases, the geometry about the gold(III) atom was, as expected, square planar. The metrical parameters of **1** are, within experimental error, identical to those previously reported.¹⁷ In complexes **3** and **4**, the gold(III) atom is bound by two phosphorus atoms

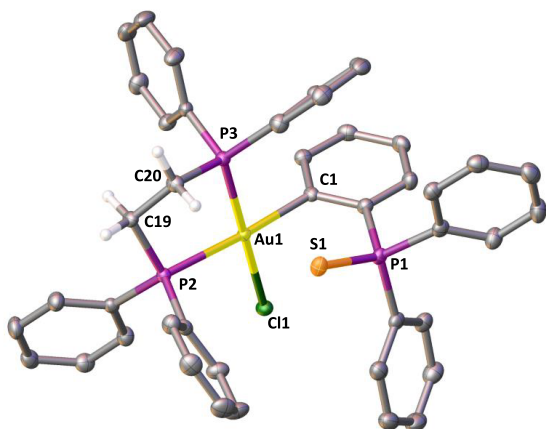


Figure 4. Molecular structure of $[\text{AuCl}(\text{dppe})\{\kappa\text{C}-2\text{-C}_6\text{H}_4\text{P}(\text{S})\text{Ph}_2\}]\cdot\text{Cl}\cdot 0.931(\text{H}_2\text{O})\cdot 0.069(\text{CH}_2\text{Cl}_2)$ (**3**). Ellipsoids show 50% probability levels. Hydrogen atoms on the phenyl rings, chloride counterion, and solvents of crystallization have been omitted for clarity. Selected bond distances (Å) and angles (deg): Au(1)–C(1) 2.0815(16), Au(1)–P(2) 2.3904(8), Au(1)–P(3) 2.3051(7), Au(1)–Cl(1) 2.3551(7), P(1)–S(1) 1.9666(7), C(1)–Au(1)–P(2) 176.38(4), P(3)–Au(1)–Cl(1) 175.913(14).

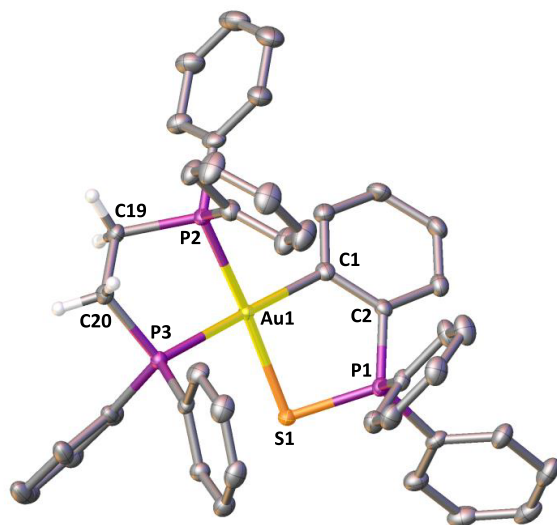


Figure 5. Molecular structure of $[\text{Au}(\text{dppe})\{\kappa^2\text{-}2\text{-C}_6\text{H}_4\text{P}(\text{S})\text{Ph}_2\}][\text{PF}_6]_2\cdot 3(\text{CH}_2\text{Cl}_2)$ (**4**). Ellipsoids show 50% probability levels. Hydrogen atoms on the phenyl rings, PF_6^- counterions, and solvent of crystallization have been omitted for clarity. Selected bond distances (Å) and angles (deg): Au(1)–C(1) 2.090(4), Au(1)–P(3) 2.3830(13), Au(1)–P(2) 2.3141(12), Au(1)–S(1) 2.3756(11), S(1)–P(1) 2.0340(16), C(1)–Au(1)–P(3) 178.01(14), P(2)–Au(1)–S(1) 171.71(6).

of the dppe ligand, the carbon atom of the $\text{C}_6\text{H}_4\text{P}(\text{S})\text{Ph}_2$ ligand, and either a chlorine (complex **3**) or sulfur (complex **4**) atom. As expected, the Au–P bond length *trans* to the carbon atom of the $\text{C}_6\text{H}_4\text{P}(\text{S})\text{Ph}_2$ group (*ca.* 2.38 Å) is significantly longer than the Au–P bond length *trans* to chloride or sulfur (*ca.* 2.30 Å), consistent with the higher *trans* influence of σ -carbon ligands.

Interactions with Human Serum Albumin. Human serum albumin (HSA) is a major plasma protein and comprises ~55% of the whole blood plasma proteins. HSA increases the solubility of drugs, including metal complexes, in plasma and plays an important role in their cellular uptake and pharmacokinetics. The intrinsic emissive properties of the tryptophan residue in HSA is very sensitive to changes in the microenvironment of the protein.¹⁹ Therefore, we investigated the binding interactions of complexes **1–4** with HSA by fluorescence spectroscopy. The fluorescence emission spectra of HSA in PBS were acquired in the absence and presence of different concentrations of complexes **1–4** (Figure 6A and Figure S13), and a decrease in the characteristic emission maximum of HSA at 346 nm was observed with increasing concentrations of the complexes. Notably, the maximum emission wavelength did not change during the interaction with the complexes and combined with the decrease in intensity, indicated a reduction in the polarity of the microenvironment as a result of the complexes binding to the hydrophobic cavity of the protein.²⁰ The interaction of complexes **1–4** with HSA resulted in a quenching of the fluorescence by 54.4, 19.7, 50.1, and 38.2%, respectively (Figure 6B).

A better understanding of the HSA fluorescence quenching mechanism by the gold compounds can be obtained using Stern–Volmer equations. As shown in Figure 6C, the Stern–Volmer plots (F^0/F versus concentration of the compounds) exhibited linear relationships and the Stern–Volmer quenching constants (K_{SV}) were obtained from the slope of these linear plots using the equation $F^0/F = 1 + K_{\text{SV}}[Q]$, where F and F^0 are the fluorescence intensity of HSA in the presence and absence of the gold compounds, respectively. The binding constants (K_b) and number of binding sites (n) were obtained from the intercept and slopes of Scatchard plots $\log(F^0 - F)/F$ vs $\log[Q]$ (Figure 6D) using the equation $\log(F^0 - F)/F = \log K_b + n \log[Q]$. The values are summarized in Table S1. The results show that the calculated K_q values for the gold compounds were higher than the K_q of quencher with biopolymers ($2.0 \times 10^{10} \text{ M}^{-1} \text{ s}^{-1}$) suggesting a static quenching mechanism is involved in the HSA fluorescence quenching. Further, the values of K_b indicate a higher binding affinity of compound **2** to HSA, followed by compounds **3**, **1**, and **4**. It was also observed that the values of n were approximately equal to 1, suggesting a single binding site for the metal complexes in the HSA molecule.

Stability of the Gold Complexes in Dimethyl Sulfoxide (DMSO) and Physiological-Like Conditions.

Previous studies have reported that gold complexes are vulnerable to ligand exchange and reduction reactions in DMSO and physiological conditions.^{1,21} Therefore, the stability of complexes **1–4** in d_6 -DMSO and cell culture medium (Roswell Park Memorial Institute, RPMI medium) was monitored by ^{31}P NMR spectroscopy (Figures S9–S12) and UV–vis spectroscopy (Figure 7), respectively. Complexes **1** and **2** were stable in DMSO solution, even after 72 h, and no significant changes in their NMR spectra were observed. In

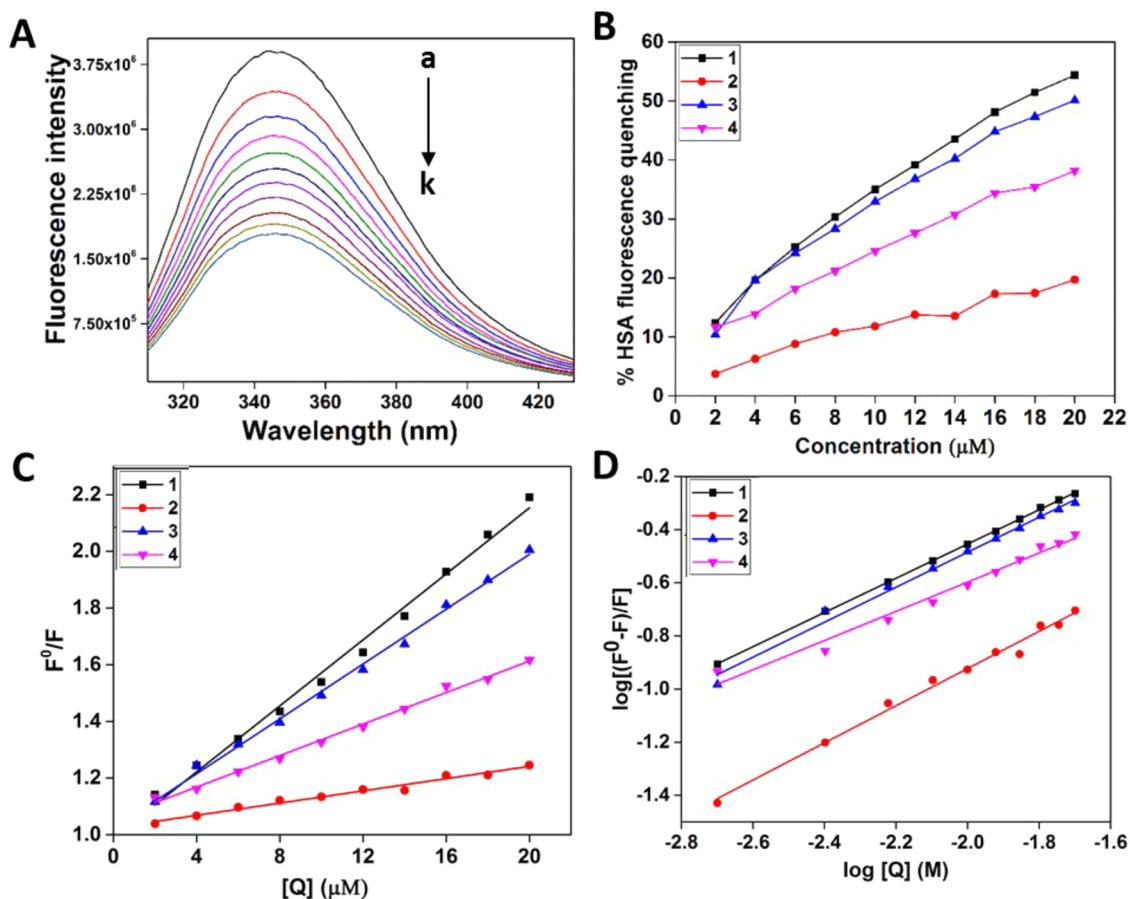


Figure 6. Interaction between the gold(III) complexes and HSA studied by fluorescence spectroscopy. (A) The fluorescence emissions of HSA (10 μM) were recorded in the absence and presence of complex 1, with increasing concentrations (0, 2, 4, 6, 8, 10, 12, 14, 16, 18, and 20 μM) from a to k. (B) Percentage of fluorescence quenching after treatment with different concentrations of complexes 1–4. (C) Stern–Volmer plots of quenching of HSA fluorescence by the gold compounds 1–4. (D) Scatchard plots of the fluorescence titrations of the gold compounds 1–4 with HSA.

contrast, complexes 3 and 4 were only stable for ca. 2 h before evidence for the formation of new species was evident. Complex 3 slowly but cleanly gave a new species, as shown by the appearance of peaks at δ 42.3, 34.0, and 29.3 in the ³¹P NMR spectrum, tentatively identified as [Au(DMSO)(dppe)-{ κ C-2-C₆H₄P(S)Ph₂}]Cl₂. Attempts to obtain X-ray quality crystals of this species were unsuccessful. In contrast to 3, solutions of 4 slowly gave a complex mixture of species which could not be identified. In agreement with the NMR spectroscopic results above, complexes 1 and 2 showed no significant time-dependent UV–vis spectral changes in cell culture medium, indicating that the complexes are stable under physiological-like conditions. Further, complexes 3 and 4 showed a slight decrease in absorbance over an incubation period of 72 h (Figure 7).

In Vitro Cytotoxicity. Preliminary *in vitro* cytotoxicity studies on the gold complexes were conducted to investigate their anticancer activity against cervical (HeLa), lung (A549), prostate (PC3), fibrosarcoma (HT1080), and breast (MDA-MB-231) cancer cells. The compounds were also tested for their cytotoxicity toward human umbilical vascular endothelial cells (HUVEC), which were employed as a noncancerous cell model. IC₅₀ values were calculated from dose response curves obtained after 72 h of exposure of the compounds using the MTT assay, and the results were compared with the clinically used drug cisplatin. As shown in Table 1, all the gold compounds showed higher potency against HeLa, HT1080,

and MDA-MB-231 cells than cisplatin; compounds 2, 3, and 4 showed similar cytotoxicity and potency toward the three cell lines with IC₅₀ values in the range 0.17–2.50 μM and exhibited approximately 8-, 3–6-, 3–5-, and 3–12-fold higher cytotoxicity than cisplatin against HeLa, PC3, HT1080, and MDA-MB-231 cancer cells, respectively. Among the series, compound 2 showed the highest selectivity toward cancer cells followed by compound 1. For instance, compound 2 exhibited 9-, 15- and 5-fold higher selectivity toward HeLa, HT1080, and MDA-MB-231 cells, respectively, compared to noncancerous HUVEC cells.

Cellular Uptake. As the biological activity of the compounds is determined by the extent of cellular accumulation,²² flow cytometric analysis of cells pretreated with increasing concentrations (0.5, 1, and 2 μM) of complexes 1–4 was undertaken. In all cases, a characteristic shift in the side scatter pattern (SSC) owing to increased cellular granularity was observed. The greatest shift was observed for compound 2 and is concentration-dependent, indicating its efficient uptake (Figure 8A). We also investigated the amount of gold taken up by the cells using ICP-MS. HeLa cells were treated with equimolar concentrations of compounds 1–4 (1 μM) for 12 h, and the total cellular accumulation of gold was determined. As shown in Figure 8B, cells treated with complexes 2–4 showed higher levels of gold uptake than those treated with 1 and correlate with the cytotoxic potency of the compounds (Table 1).

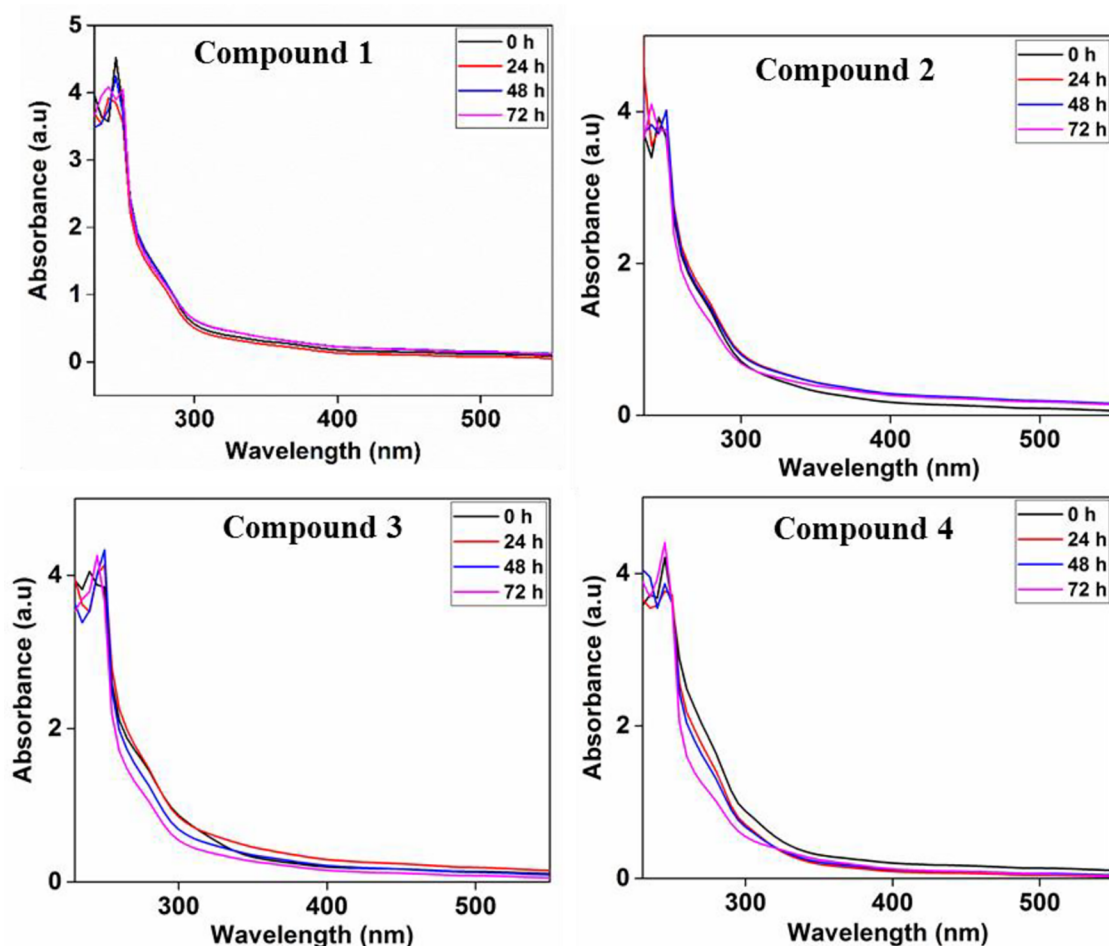


Figure 7. Electronic absorption spectra of gold complexes 1–4 (20 μM) in complete growth medium (RPMI) over a period of 72 h.

Table 1. *In Vitro* Anticancer Activity (IC_{50} , μM) of the Newly Synthesized Gold Complexes 1–4 and Cisplatin against a Panel of Cancerous and Noncancerous Cells^a

compound	HeLa	A549	PC3	HT1080	MDA-MB- 231	HUVEC
1	1.15 \pm 0.09	>50	2.41 \pm 0.14	9.11 \pm 0.78	17.41 \pm 1.63	5.26 \pm 0.15
2	0.42 \pm 0.07	6.97 \pm 0.32	1.01 \pm 0.21	0.26 \pm 0.06	0.73 \pm 0.05	3.89 \pm 0.32
3	0.36 \pm 0.12	2.60 \pm 0.47	1.65 \pm 0.16	0.21 \pm 0.05	0.54 \pm 0.08	0.93 \pm 0.16
4	0.46 \pm 0.03	6.08 \pm 0.48	2.45 \pm 0.11	0.17 \pm 0.04	2.50 \pm 0.09	2.13 \pm 0.19
cisplatin	3.25 \pm 0.11	5.69 \pm 0.37	6.31 \pm 0.06	0.63 \pm 0.06	6.35 \pm 0.51	6.89 \pm 1.23

^aHeLa, cervical cancer cells; A549, lung cancer cells; PC3, prostate cancer cells; HT1080, fibrosarcoma; MDA-MB-231, breast; HUVEC, human umbilical vascular endothelial cells.

TrxR Inhibition. Although the exact mechanism of action for the anticancer activity of many gold complexes has yet to be elucidated, the high affinity of gold compounds to undergo facile ligand exchange reactions with sulfur- and selenium-containing groups in thioredoxin reductase (TrxR) makes this enzyme a compelling molecular target.²³ The thioredoxin (TrxR) system plays a key role in cellular homeostatic processes which neutralize reactive oxygen species (ROS) and helps to overcome cellular oxidative stress.²⁴ Therefore, the inhibition of TrxR has recently emerged as an attractive strategy in cancer treatment.^{25,26} In this regard, we investigated the TrxR inhibition ability of compounds 1–4 using the lipoate reduction assay.²⁷ The results, shown in Figure 9, indicate that treatment of HeLa cells with 1–4 leads to a strong inhibition of TrxR in a concentration-dependent manner. Relative to the vehicle control, the greatest inhibition

was observed for compound 1 followed by compounds 2, 4, and 3. The higher TrxR inhibition in 1 may be due to participation in ligand exchange reactions between the chloride ligands and the selenocysteine residue in TrxR. These results are in contrast with the growth inhibition values, where compounds 2–4 are more cytotoxic than compound 1, suggesting compounds 2–4 may have other cellular targets.

Gold Compound-Induced ROS Production in HeLa Cells. It has been reported that inhibition of the antioxidant TrxR enzyme may result in apoptosis induction in cancer cells through increased ROS accumulation.²⁸ Therefore, we investigated whether TrxR inhibition led to ROS accumulation in HeLa cells. The intracellular levels of ROS in HeLa cells after treatment with the gold complexes were analyzed using carboxy- H_2DCFDA . After being taken up by cells, the nonfluorescent DCFDA is oxidized to fluorescent dichloro-

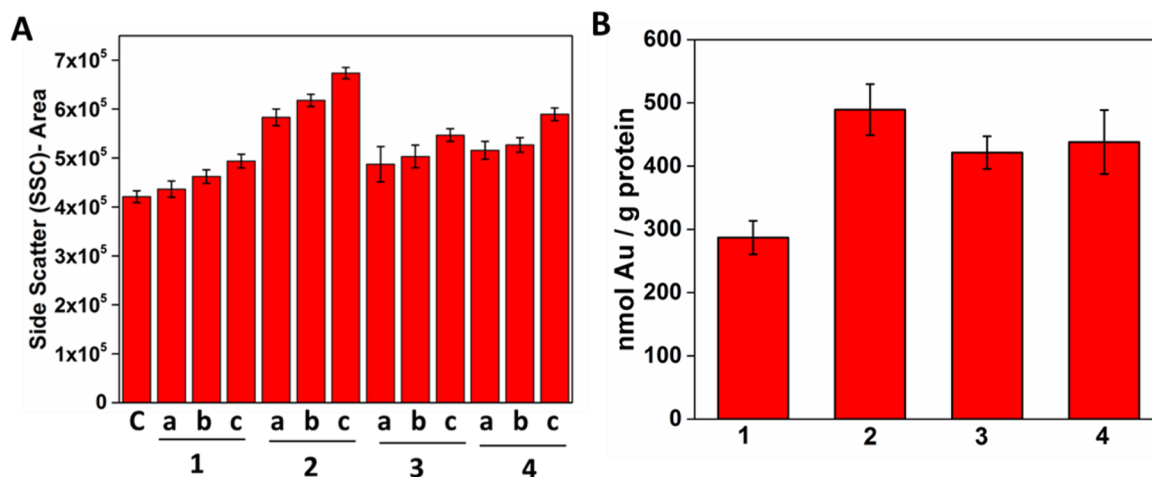


Figure 8. Determination of intracellular accumulation of gold compounds 1–4. (A) Side scatter analysis of HeLa cells after treatment with 0.5, 1, and 2 μM concentrations of the gold complexes for 12 h. (B) HeLa cells were treated with 1 μM gold compounds for 12 h, and the amount of intracellular gold was determined by ICP-MS. The data represent the mean \pm the standard deviation of three independent experiments.

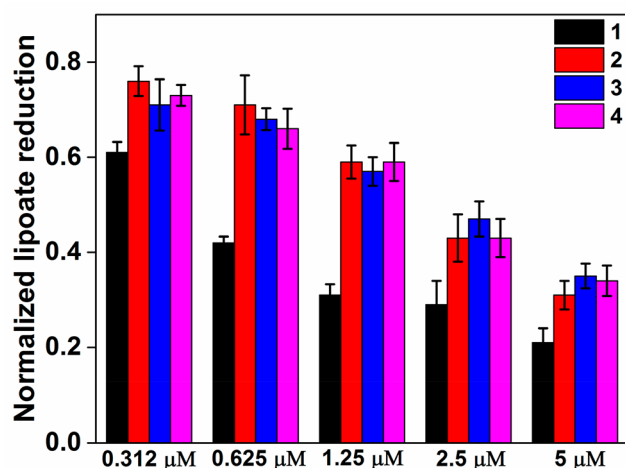


Figure 9. TrxR inhibition in HeLa cells treated with different concentrations of compounds 1–4 for 6 h and monitored colorimetrically for lipote reduction.

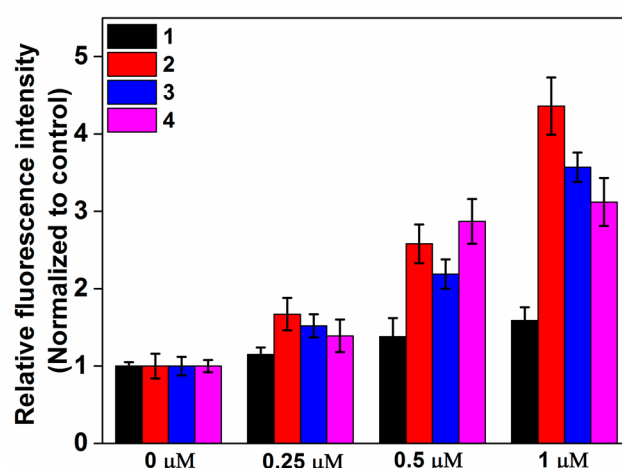


Figure 10. Accumulation of reactive oxygen species in HeLa cells. HeLa cells treated with gold compounds 1–4 (0, 0.25, 0.5, and 1 μM) for 6 h were further incubated with carboxy- H_2DCFDA (10 μM) for 30 min. The bar chart shows the fluorescence intensity values compared to the untreated controls.

fluorescein (DCF) by the action of cellular ROS,²⁹ and thus the fluorescence intensity of DCF is directly proportional to ROS levels.

As shown in Figure 10, treatment of HeLa cells with compounds 1–4 led to increased intracellular ROS accumulation. Among the series, treatment with compound 2 resulted in the greatest accumulation of ROS in a concentration-dependent manner. The intracellular ROS levels were increased to significant levels when the cells were treated with 1 μM of compound 2 (4.3-fold increase), correlating with the high cytotoxicity of this compound.

Wound Healing Assay. The migration of endothelial cells to form a blood supply network is essential for the progression of tumors and metastasis.³⁰ Therefore, the discovery of drugs that can inhibit both cancer cell growth and endothelial cell motility is essential for efficient cancer therapy. In this regard, we investigated the ability of the gold complexes to inhibit the migration ability of highly migratory human umbilical vascular endothelial cells (HUVEC) using a wound healing assay.³¹

As shown in Figure 11, the linear scratch assay shows the rapid migration of the control cells into the wounded area

while the wells treated with compounds 1–4 showed fewer cells migrating to the scratched area. The wound closure followed the order control > 1 > 4 > 3 > 2. These results thus underpin the excellent migration inhibition abilities of compound 2 in HUVEC lines.

Tube Formation and Angiogenesis Assay. It has been reported that TrxR inhibition by metal complexes may contribute to the inhibition of the angiogenesis process, which plays an important role in the development and spread of tumors from benign to malignant.³² Therefore, the antiangiogenic effect of the synthesized compounds was investigated by observing tube formation of HUVECs in matrigel constructs.³³ Elongated, robust networks of HUVECs were clearly seen in wells seeded with untreated cells, whereas network formation was significantly inhibited when cells were treated with compounds 1–4 (Figure 12 and Figure S14). Quantification of tube formation using WimTube showed that all aspects of network formation were significantly affected in complex-treated wells, as indicated by a decrease of cell-

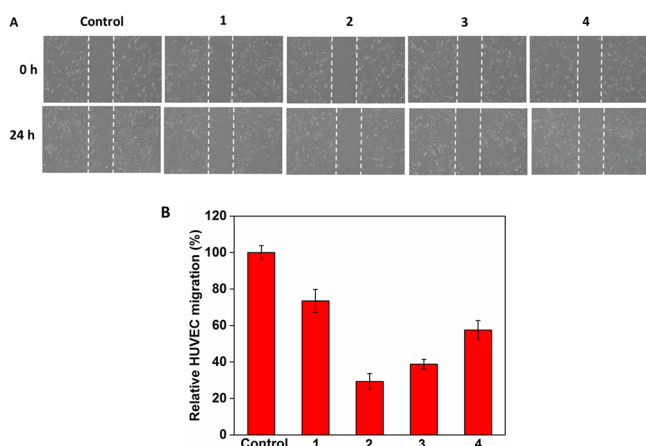


Figure 11. Wound healing assay. Wounds created in HUVEC monolayers. Cells were treated with IC_{50} concentrations of compounds 1–4 for 24 h. (A) Images of wounds captured immediately (0 h) and 24 h after treatment and viewed at 4 \times magnification. (B) The number of cells migrated into the wound area was counted manually. Data are the mean \pm the standard deviation from three independent experiments.

covered area, number of tubes and branching points, and total length of tubes, highlighting the excellent antiangiogenic properties of the complexes.

In Vivo Antitumor Activity. The excellent *in vitro* cytotoxicity, cellular uptake, antimigratory, and angiogenesis inhibition properties of compound 2 prompted us to investigate the *in vivo* activity in nude mice. To test the *in vivo* tumor growth inhibition efficacy, experiments were conducted on female BALB/c nude mice bearing human cervical tumor xenografts. Cisplatin was used as positive standard. Nude mice bearing HeLa xenografts were treated with intraperitoneal injections of compound 2 (1 mg/kg), cisplatin (1 mg/kg), or vehicle control every 3 days for 42 days. As shown in Figure 13A and B, an exponential increase in tumor volume over time was observed in the control mice, but mice treated with the metal complexes showed tumor growth inhibition. At the end of the experiment, tumor growth inhibition was significant for mice treated with compound 2 (55%) compared to those treated with cisplatin (28%).

We also analyzed the tumor tissues for the expression of Ki-67, a cell proliferation marker, by immunohistochemistry.³⁴ As shown in Figure 13C and D, treatment with the gold compounds resulted in an approximately 50% reduction in Ki-67 positive cells, whereas cisplatin treated mice showed 45% lower Ki-67 positive cells, indicating the gold complexes inhibited tumor proliferation. By comparison to the results of the control mice, there were no significant morphological changes in the kidney and liver tissues of the mice treated with compound 2 (Figure 13C–E). In addition, no mouse death or

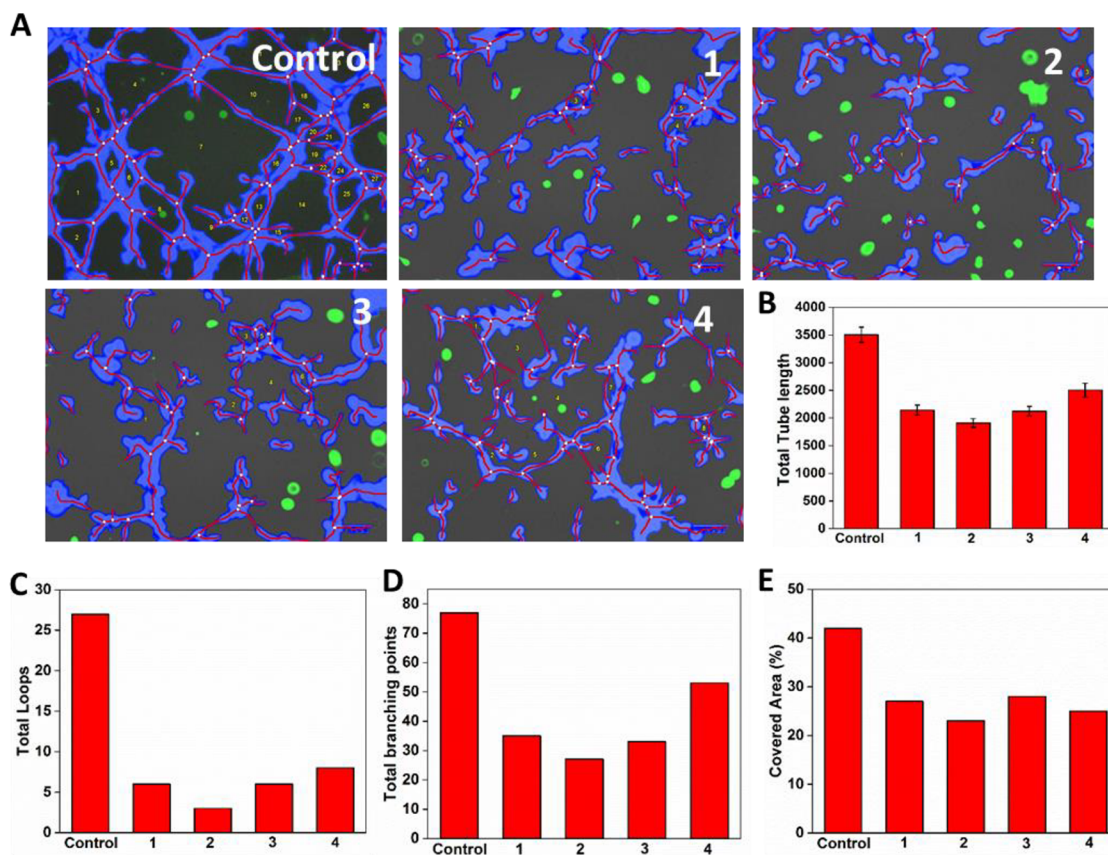


Figure 12. Tube formation of HUVEC cells. HUVECs cultured on matrigel coated plates were treated with IC_{50} concentrations of compounds 1–4 for 16 h. (A) Morphological changes and tube formation were visualized by microscopy, and representative images are shown. The total lengths of the tubes, loops, branching points, and covered area in the presence and absence of the gold compounds were analyzed and are shown in the bar graphs B–E, respectively.

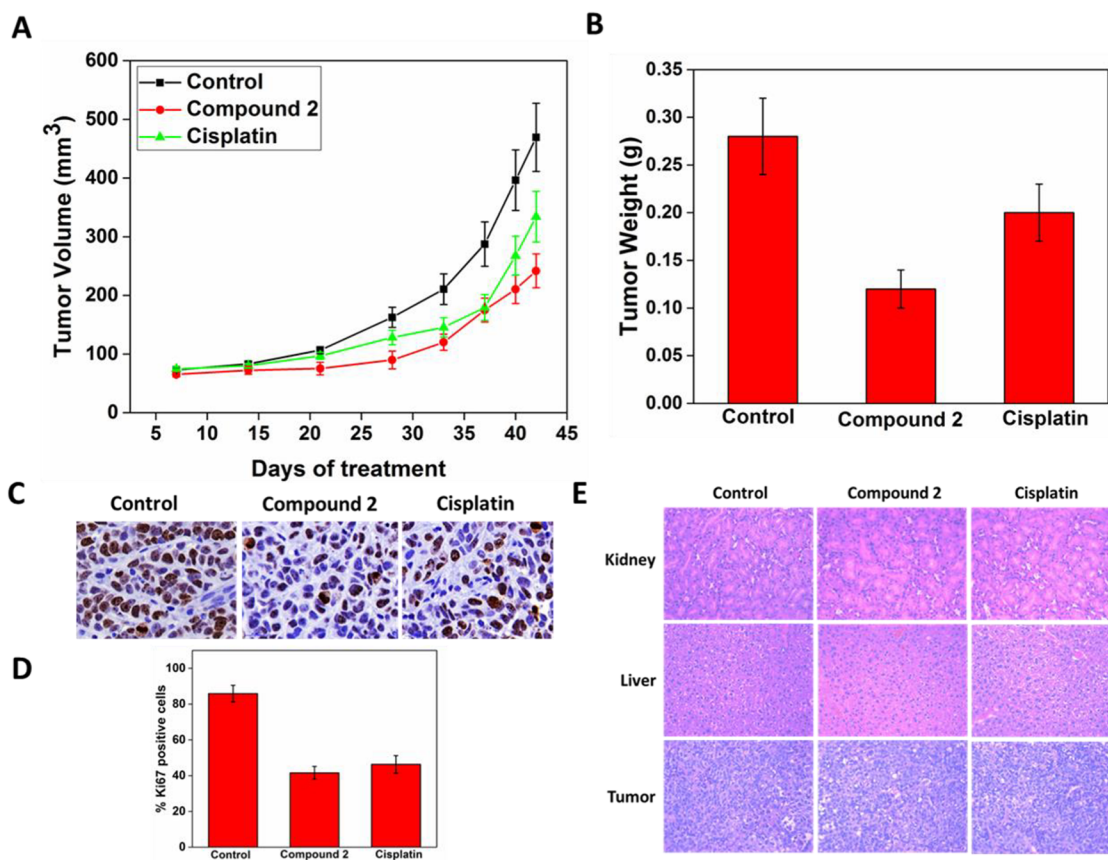


Figure 13. *In vivo* antitumor activity of gold compound 2 and cisplatin. BALB/c nude mice bearing HeLa xenografts received intraperitoneal injections of either metal complexes (1 mg/kg) or vehicle control (DMSO; $n = 5$) every 3 days. (A) Tumor volumes were measured at different time points with vernier calipers and are expressed with \pm standard error. (B) Isolated tumor weights. (C) Representative images of the immunohistochemical staining of the proliferation marker Ki-67. (D) Quantification of cells positive for Ki-67 (as a % of control). (E) Haematoxylin and eosin staining of isolated kidney, liver, and tumor tissues. A standard Student's t test was used for statistical analysis to determine statistically significant differences with respect to the control. * $p < 0.01$. ** $p < 0.001$.

change in body weight was observed in any of the mice throughout the experiments, suggesting no general toxicity.

CONCLUSION

A series of cycloaurated gold(III) complexes derived from triphenylphosphine sulfide have been prepared and their anticancer properties investigated toward a panel of five different human tumor cell lines. Among the complexes, $[\text{AuCl}_2\{\kappa^2\text{-}2\text{-C}_6\text{H}_4\text{P}(\text{S})\text{Ph}_2\}]$ (**1**) and $[\text{Au}(\kappa^2\text{-S}_2\text{CNEt}_2)\{\kappa^2\text{-}2\text{-C}_6\text{H}_4\text{P}(\text{S})\text{Ph}_2\}]\text{PF}_6$ (**2**) demonstrated outstanding stability in solution even after 72 h. Compounds **2**–**4** were found to be the most cytotoxic against various cancer cell lines with high selectivity and almost on par with the commercially used anticancer drug cisplatin. The compounds also showed excellent inhibition of endothelial cell migration with antiangiogenic activity. In cervical cancer cells, the mechanism of anticancer activity for complex **2** involved apoptotic cell death through increased production of ROS. Compound **2** also showed effective *in vivo* anticancer activity toward cervical tumor xenografts in nude mice with no observable general toxicity. The superior activity of **2** relative to the other complexes studied may be due to several factors. For example, replacement of the two chloride ligands in the coordination sphere of $[\text{AuCl}_2\{\kappa^2\text{-}2\text{-C}_6\text{H}_4\text{P}(\text{S})\text{Ph}_2\}]$ by a dithiocarbamate ligand increases the lipophilicity of the complex, evidenced by the greater cellular uptake of **2** (495 nmol Au/g protein)

compared to that of **1** (280 nmol Au/g protein). Additionally, the bidentate dithiocarbamate ligand confers stability to the complex due to significant contribution of the dithiolate canonical form $\text{Et}_2\text{N}^+=\text{CS}_2^{2-}$ and is more labile than the bidentate diphosphine ligand dppe for easier participation in exchange reactions with cellular enzymes. The present work highlights the promising prospects of cycloaurated gold(III) complexes in the development of new drug molecules for cancer treatment.

EXPERIMENTAL SECTION

Chemistry. $[\text{Bu}_4\text{N}][\text{AuCl}_4]$, $2\text{-Me}_3\text{SnC}_6\text{H}_4\text{P}(\text{S})\text{Ph}_2$, and $\text{Na}_2\text{S}_2\text{CNEt}_2 \cdot 3\text{H}_2\text{O}$ were prepared according to literature methods.^{36–38} ^1H (300 MHz) and ^{31}P (121 MHz) NMR spectra were acquired in d_6 -DMSO, unless stated otherwise, on a Bruker Avance 300 spectrometer at room temperature. Chemical shifts are referenced to residual solvent signals (^1H) or external 85% H_3PO_4 (^{31}P), and coupling constants (J) are given in Hz. Mass spectra were acquired on a Bruker Autoflex Speed (MALDI) or PerkinElmer Axion 2 TOF (ESI) spectrometer. Elemental analyses were performed by the Microanalytical Unit of the Department of Molecular Sciences at Macquarie University, Sydney.

X-ray Crystallography. Crystals of complexes **1**, **3**, and **4** suitable for single-crystal X-ray diffraction were obtained from dichloromethane/hexane (**1**) or dichloromethane/ether (**3** and **4**). Using a drop of inert oil (Paratone), crystals were mounted on a nylon loop and transferred to a stream of cold nitrogen. The reflections were collected on a D8 Bruker diffractometer equipped with an APEX-II

area detector using graphite monochromated Mo $K\alpha$ radiation ($\lambda = 0.71073 \text{ \AA}$) from a $1 \mu\text{S}$ microsource. The computer programs SMART³⁹ and SAINT⁴⁰ were used for data collection in φ - and ω -scan modes and data processing, respectively, and absorption corrections using SADABS.⁴¹ The structures were solved using direct methods and refined with full-matrix least-squares methods on F^2 using the SHELX-TL package.^{42,43} The CCDC numbers for complexes 1, 3, and 4 are 1883144–1883146.

Preparation of $[\text{AuCl}_2\{\kappa^2\text{-}2\text{-C}_6\text{H}_4\text{P(S)Ph}_2\}]$ (1). A bright yellow solution of $[\text{Bu}_4\text{N}][\text{AuCl}_4]$ (1.03 g, 1.77 mmol) and 2-Me₃SnC₆H₄P(S)Ph₂ (810 mg, 1.77 mmol) in CH₂Cl₂ (20 mL) was left to stir in the dark overnight. Hexane was added to the resulting pale-yellow solution, and the volume was reduced *in vacuo*, precipitating out a pale yellow solid. The solid was isolated by filtration, washed sequentially with hexane and MeOH, then recrystallized from CH₂Cl₂/MeOH to give the title compound (933 mg, 94%). ¹H NMR: δ 7.36 (dd, $J = 1.8, 11.7 \text{ Hz}$, 1H), 7.47 (ddt, $J = 1.0, 4.4, 7.4 \text{ Hz}$, 1H), 7.54–7.61 (m, 1H), 7.72–7.94 (m, 10H), 8.21 (ddd, $J = 1.0, 3.4, 8.2 \text{ Hz}$, 1H). ³¹P NMR: δ 56.1 (s). HR-ESI MS (m/z): 524.9856. Calcd for C₁₈H₁₄AuClPS: 524.9908 [M – Cl]⁺. Elem anal. calcd for C₁₈H₁₄AuCl₂PS: C, 38.52; H, 2.51; S, 5.71. Found: C, 38.46; H, 2.33; S, 5.77.

Preparation of $[\text{Au}(\kappa^2\text{-S}_2\text{CNET}_2)\{\kappa^2\text{-}2\text{-C}_6\text{H}_4\text{P(S)Ph}_2\}]\text{PF}_6$ (2). To a solution of 1 (100 mg, 0.18 mmol) in CH₂Cl₂ (10 mL) was added Na₂S₂CNET₂·3H₂O (50 mg, 0.18 mmol). The pale-yellow solution darkened slightly and was stirred for 10 min. TlPF₆ (130 mg, 0.37 mmol) was added to the solution, which was stirred for 1 h in the dark. The suspension was filtered through Celite, and hexane was added to the filtrate. The volume of the solution was reduced *in vacuo*, precipitating out a pale yellow solid, which was filtered off, washed with hexane, and dried *in vacuo* (126 mg, 90%). ¹H NMR: δ 1.29 (br. m, 6H), 3.83 (br. m, 4H), 7.42–8.00 (m, 14H). ³¹P NMR: δ 61.1 (s), –144.2 (sept, $J = 711 \text{ Hz}$). HR-ESI MS (m/z): 638.0431. Calcd for C₂₃H₂₄AuNP₃S₃: 638.0474 [M – PF₆]⁺. Elem anal. calcd for C₂₃H₂₄AuF₆NP₃S₃·0.5H₂O: C, 34.86; H, 3.18; N, 1.77; S, 12.14. Found: C, 34.65; H, 2.86; N, 1.85; S, 13.02.

Preparation of $[\text{AuCl}(\text{dppe})\{\kappa^2\text{-}2\text{-C}_6\text{H}_4\text{P(S)Ph}_2\}]\text{Cl}$ (3). To a solution of 1 (100 mg, 0.18 mmol) in CH₂Cl₂ (10 mL) was added dppe (71 mg, 0.18 mmol). After stirring for 5 min, the volume of the solution was reduced to ~3 mL and Et₂O added dropwise, precipitating out a pale yellow solid. The solid was isolated by filtration, washed with Et₂O, and dried *in vacuo* (157 mg, 92%). ¹H NMR: δ 3.60–3.89 (br. m, 2H), 6.84–8.11 (m, 34H). Two methylene protons are obscured by the water peak at δ 3.4. ³¹P NMR: δ 61.1 (d, $J = 4.6 \text{ Hz}$), 52.1 (dd, $J = 4.7, 20 \text{ Hz}$), 45.0 (d, $J = 20 \text{ Hz}$). ¹H NMR (CDCl₃): δ 3.28–3.51 (br. m, 2H), 3.93–4.03 (br. m, 2H), 6.81–7.16 (m, 6H), 7.27–7.73 (m, 24H), 7.96–8.03 (m, 4H). MALDI MS (m/z): 919.2. Calcd for C₄₅H₄₁AuOP₃S: 919.2 [M – 2Cl + OCH₃]⁺ (from MeOH). HR-ESI MS (m/z): 914.1591. Calcd for C₄₅H₃₈AuNP₃S: 914.1603 [M – 2Cl + CN]⁺ (from MeCN). Elem anal. calcd for C₄₄H₃₈AuCl₃P₃S·1.5H₂O: C, 53.56; H, 4.19; S, 3.25. Found: C, 53.47; H, 3.99; S, 3.33.

Preparation of $[\text{Au}(\text{dppe})\{\kappa^2\text{-}2\text{-C}_6\text{H}_4\text{P(S)Ph}_2\}]\text{PF}_6$ (4). To a solution of 1 (100 mg, 0.18 mmol) in CH₂Cl₂ (10 mL) was added dppe (71 mg, 0.18 mmol) followed by TlPF₆ (140 mg, 0.40 mmol). The suspension was stirred in the dark for 1 h, then filtered through Celite. Hexane was added to the filtrate, and the volume of the solution was reduced *in vacuo*, precipitating out a colorless solid. The solid was isolated by filtration, washed with hexane, and dried *in vacuo* (194 mg, 92%). ¹H NMR: δ 3.18–3.30 (m, 2H), 3.59–3.77 (m, 2H), 6.67–6.80 (m, 1H), 7.14–7.23 (m, 1H), 7.33–7.88 (m, 30H), 7.92–8.02 (m, 2H). ³¹P NMR: δ 77.0 (s), 65.0 (d, $J = 39 \text{ Hz}$), 59.8 (d, $J = 38 \text{ Hz}$), –144.2 (sept, $J = 711 \text{ Hz}$). MALDI MS (m/z): 919.4. Calcd for C₄₅H₄₁AuOP₃S: 919.2 [M – 2(PF₆) + OCH₃]⁺ (from MeOH). Elem anal. calcd for C₄₄H₃₈AuF₁₂P₃S: C, 44.84; H, 3.25; S, 2.72. Found: C, 44.79; H, 3.29; S, 3.09.

Interactions with Human Serum Albumin. HSA solutions in PBS (10 μM) were freshly prepared before performing the experiments. The fixed concentration of HSA was titrated with different concentrations of each gold complex (2–20 μM). The HSA

solutions with or without metal complexes were incubated for 5 min and their emission spectra recorded ($\lambda_{\text{ex}} = 295 \text{ nm}$, $\lambda_{\text{em}} = 300\text{--}450 \text{ nm}$) using a cuvette of 1 cm path length.

Biological Methods. Cell culture supplements, media, Hoeschst 33242, and Carboxy-DCFDA were purchased from Invitrogen. Ten millimolar stock solutions of the metal complexes were prepared in DMSO.

Cell Culture. Human cervical (HeLa), prostate (PC3), lung (A549), and breast (MDA-MB-231) cancer cell lines were grown at 37 °C in a humidified 5% CO₂ atmosphere in RPMI medium supplemented with 10% heat-inactivated fetal bovine serum (FBS), penicillin (100 U/mL), and streptomycin (100 $\mu\text{g}/\text{mL}$). Fibrosarcoma (HT1080) cells were grown in Dulbecco's modified Eagle's medium (DMEM) supplemented with 10% FBS, penicillin (100 U/mL), and streptomycin (100 $\mu\text{g}/\text{mL}$). HUVEC cells were grown in M200 medium supplemented with low serum growth supplement (LSGS). 0.05% Trypsin-EDTA was used for detaching the cells from the culture flasks.

Cell Viability Assay. The *in vitro* cytotoxicity of the metal complexes was evaluated using the MTT [3-(4,5-dimethylthiazol-2-yl)-2,5-diphenyltetrazolium bromide] assay. Briefly, 3000 to 5000 cells were seeded in 96 well plates, dependent upon the doubling time of the cell line, and were allowed to adhere at 37 °C in a 5% CO₂ atmosphere. After overnight incubation, the medium was removed and replaced with fresh media containing different concentrations of the metal complexes. Next, 0.5% DMSO was used as a vehicle control. After 72 h of treatment, 10 μL of a 5 mg/mL MTT solution was added to each well, and the cells were incubated for 4 h. Unreacted MTT was removed, and 100 μL of DMSO was added to each well to solubilize the obtained formazan crystals. The absorbance of each well was recorded using a plate reader (Spectra Max) at 570 nm and is proportional to the number of viable cells. Therefore, percentage inhibition of cell growth at each tested concentration was determined using the formula % inhibition = 100 × (control absorbance – sample absorbance). Dose response curves were plotted, and IC₅₀ values were calculated using plot software.

Cellular Uptake. HeLa cells (1×10^6) were seeded in 25 cm² flasks in 5 mL of complete growth medium and allowed to adhere for 24 h. The cells were treated with different concentrations (0.5, 1, and 2 μM) of gold complexes for 12 h and were collected by trypsinization. The collected cells were washed with PBS and analyzed by flow cytometry (BDC6-Accuri).

For ICP-MS measurements, cells treated with 1 μM concentrations of the gold complexes were harvested with trypsin-EDTA. The collected cell pellets were lysed with lysis buffer, and each sample was divided into two portions. One aliquot was used to determine the protein content in each sample using the bicinchoninic acid (BCA) protein assay. The second aliquot was digested with HNO₃ at 65 °C for 3 h. After cooling, the mineralized sample was diluted to 10 mL with ultrapure water. The gold content was determined by axial ICP-MS (PerkinElmer).

TrxR Inhibition. In this assay, the ability of HeLa cells to reduce the cell permeable cofactor (lipoate) was monitored colorimetrically after 6 h of treatment with compounds 1–4. HeLa cells (10 000 cells/well) seeded in 96 well plates were incubated with compounds 1–4 (0.312, 0.625, 1.25, 2.5, and 5 μM) for 6 h at 37 °C. After incubation, the growth medium containing the gold compounds was replaced with 100 μL of reaction mixture (20 mM lipoate and 1 mM DTNB) in HBSS (Hanks balanced salt solution). The plates were monitored immediately and after 180 min for a change in absorbance at 405 nm due to the reduction of DTNB using a microplate reader (SpectraMax).

ROS Production. The levels of intracellular ROS were determined using the ROS-sensitive probe carboxy-DCFDA (Molecular Probes-Invitrogen). Briefly, HeLa cells seeded in 24 well plates in RPMI 1640 were treated with IC₅₀ concentrations of the gold compounds for 6 h. The cells were collected with trypsin-EDTA, washed with PBS, and incubated with 10 μM of carboxy-DCFDA for 30 min at 37 °C. After incubation, the cells were washed with PBS, and the fluorescence increase of DCFDA was measured utilizing the wavelengths of 485

nm (excitation) and 527 nm (emission) in a plate reader (Spectramax).

Wound Healing Assay/Scratch Assay. HUVEC cells were seeded in a 6 well plate (1×10^5 cells/well) in M200 medium supplemented with low serum growth supplement (LSGS). After 24 h to facilitate cell attachment, the confluent monolayer was scratched in a single straight line using a sterile 200 μ L plastic pipet tip to create a wounded, cell-free area. The wells were washed with PBS and the media containing either the vehicle (0.3% DMSO) or IC₅₀ concentrations of the metal compounds was added. The cells were constantly monitored, and images were taken at 0 and 24 h to observe the migration of cells across the wounded area. The number of cells in the wounded area was counted manually, and the total number of cells was normalized against the untreated wells containing the highest number of cell migration. All the experiments were repeated thrice with triplicate samples in each set of experiments.

Tube Formation Assay. BD Matrigel (BD Bioscience, Heidelberg, Germany) was thawed at 4 °C overnight prior to the coating of matrigel in a 96 well plate. The plates were placed on ice prior to the coating, and 50 μ L of matrigel was slowly added to each well with constant, gentle agitation for an even layer formation. The coated plates were incubated at 37 °C in a 5% CO₂ atmosphere for 1 h. The gels were overlaid with cells (10 000 HUVEC cells/well) in M200 media containing either the vehicle (0.3% DMSO) or the synthesized compounds. The plates were visualized for live cells with the aid of calcein-AM (4 μ M) after 16 h of incubation. The images for both the bright field and green channels were recorded using an inverted microscope (BIORAD) to observe the subsequent effect of the compounds on the tubular structure formation. Quantification of the tube length formation was analyzed using WimTube analysis software (Onimagin Technologies SCA, Córdoba, Spain).

In Vivo Antitumor Activity. The antitumor activity of the synthesized compounds were tested in female BALB/c nude mice by subcutaneous injection of 5×10^6 HeLa cells/100 μ L RPMI medium in both ventral flanks anterior to the hind legs using a 29-gauge insulin syringe. The mice were constantly monitored for 48 h to observe any changes in weight or adverse effects prior to treatment with the compounds. Tumor volumes of 50 mm³ were established prior to the random separation of mice into three groups comprising of 5 in each. Intraperitoneal injections of either the vehicle control, 1 mg/kg of complex 2, or cisplatin were supplied three times a week for 42 days. The tumor volume was measured eight times during the 42 day period before culling of the mice. All the tumors were collected and weighed. The obtained tumors were also checked for the extent of proliferation and hence the inhibitory effect of the gold complex by subsequent staining for the Ki-67 proliferative marker. The tumor xenografts were paraffin fixed and sectioned into 4 μ m sections using a microtome. The sections were further stained using the Ventana BenchMark Immunostainer (Ventana Medical Systems, Inc., Tucson, AZ). The sections were dewaxed, and the endogenous peroxidase activity was blocked with Ventana EZ prep and Ventana Universal 3,3'-diaminobenzidine (DAB) inhibitor, respectively. The sections were stained against the primary Ki-67 marker, which was subsequently diluted according to the manufacturer's instructions. Counterstaining was carried out with Ventana hematoxylin and bluing solution. Primary antibody staining was detected using the ultraView Universal DAB Detection Kit (Roche, Basel, Switzerland). Negative controls consisted of the tumor sections in the absence of the primary antibody, while human tonsil cells were employed as positive controls. Cells were visualized using an Aperio ImageScope (Leica Microsystems, Mount Waverley, Australia) and the related digital pathology viewing software.

■ ASSOCIATED CONTENT

SI Supporting Information

The Supporting Information is available free of charge at <https://pubs.acs.org/doi/10.1021/acs.inorgchem.0c00423>.

Figures S1–S14, Table S1 (PDF)

Accession Codes

CCDC 1883144–1883146 contain the supplementary crystallographic data for this paper. These data can be obtained free of charge via www.ccdc.cam.ac.uk/data_request/cif, or by emailing data_request@ccdc.cam.ac.uk, or by contacting The Cambridge Crystallographic Data Centre, 12 Union Road, Cambridge CB2 1EZ, UK; fax: +44 1223 336033.

■ AUTHOR INFORMATION

Corresponding Authors

Suresh K. Bhargava – Centre for Advanced Materials and Industrial Chemistry, School of Science, RMIT University, Melbourne 3001, Australia; orcid.org/0000-0002-3127-8166; Email: suresh.bhargava@rmit.edu.au

Nedaossadat Mirzadeh – Centre for Advanced Materials and Industrial Chemistry, School of Science, RMIT University, Melbourne 3001, Australia; orcid.org/0000-0002-3092-2634; Email: nedaossadat.mirzadeh@rmit.edu.au

Authors

T. Srinivasa Reddy – Centre for Advanced Materials and Industrial Chemistry, School of Science, RMIT University, Melbourne 3001, Australia; orcid.org/0000-0002-2806-4300

Steven H. Privér – Centre for Advanced Materials and Industrial Chemistry, School of Science, RMIT University, Melbourne 3001, Australia; orcid.org/0000-0001-5521-9884

Rodney B. Luwor – Department of Surgery, Royal Melbourne Hospital, University of Melbourne, Parkville 3050, Australia

Velma Ganga Reddy – Centre for Advanced Materials and Industrial Chemistry, School of Science, RMIT University, Melbourne 3001, Australia; orcid.org/0000-0001-5054-2519

Shwathy Ramesan – School of Engineering, RMIT University, Melbourne 3001, Australia

Complete contact information is available at: <https://pubs.acs.org/10.1021/acs.inorgchem.0c00423>

Notes

The authors declare no competing financial interest.

■ ACKNOWLEDGMENTS

The authors acknowledge the Micro Nano Research Facility (MNRF), RMIT University for providing the facilities to carry out cell culture experiments.

■ REFERENCES

- (1) Zou, T.; Lum, C. T.; Lok, C. N.; Zhang, J. J.; Che, C. M. Chemical biology of anticancer gold(III) and gold(I) complexes. *Chem. Soc. Rev.* **2015**, *44*, 8786–8801.
- (2) Zhang, P.; Sadler, P. J. Advances in the design of organometallic anticancer complexes. *J. Organomet. Chem.* **2017**, *839*, 5–14.
- (3) Dominelli, B.; Correia, J. D. G.; Kühn, F. E. Medicinal applications of gold(I/III)-based complexes bearing N-heterocyclic carbene and phosphine ligands. *J. Organomet. Chem.* **2018**, *866*, 153–164.
- (4) Bertrand, B.; Williams, M. R. M.; Bochmann, M. Gold(III) complexes for antitumor applications: An overview. *Chem. - Eur. J.* **2018**, *24*, 11840–11851.
- (5) Lima, J. C.; Rodriguez, L. Phosphine-gold(I) compounds as anticancer agents: General description and mechanisms of action. *Anti-Cancer Agents Med. Chem.* **2011**, *11*, 921–928.

- (6) (a) Altaf, M.; Monim-ul-Mehboob, M.; Kawde, A.-N.; Corona, G.; Larcher, R.; Ogasawara, M.; Casagrande, N.; Celegato, M.; Borghese, C.; Siddik, Z. H.; Aldinucci, D.; Isab, A. A. New bipyridine gold(III) dithiocarbamate-containing complexes exerted a potent anticancer activity against cisplatin-resistant cancer cells independent of p53 status. *Oncotarget* **2017**, *8*, 490–505. (b) Kim, J. H.; Reeder, E.; Parkin, S.; Awuah, S. G. Gold(I/III)-phosphine complexes as potent antiproliferative agents. *Sci. Rep.* **2019**, *9*, 12335. (c) Altaf, M.; Casagrande, N.; Mariotto, E.; Baig, N.; Kawde, A. N.; Corona, G.; Larcher, R.; Borghese, C.; Pavan, C.; Seliman, A. A.; Aldinucci, D.; Isab, A. A. Potent in vitro and in vivo anticancer activity of new bipyridine and bipyrimidine gold(III) dithiocarbamate derivatives. *Cancers* **2019**, *11*, 474. (d) Mármol, I.; Quero, J.; Rodríguez-Yoldi, M. J.; Cerrada, E. Gold as a possible alternative to platinum-based chemotherapy for colon cancer treatment. *Cancers* **2019**, *11*, 780.
- (7) Vela, L.; Contel, M.; Palomera, L.; Azaceta, G.; Marzo, I. Iminophosphorane-organogold(III) complexes induce cell death through mitochondrial ROS production. *J. Inorg. Biochem.* **2011**, *105*, 1306–1313.
- (8) Shaik, N.; Martínez, A.; Augustin, I.; Giovinazzo, H.; Varela-Ramírez, A.; Sanaú, M.; Aguilera, R. J.; Contel, M. Synthesis of apoptosis-inducing iminophosphorane organogold(III) complexes and study of their interactions with biomolecular targets. *Inorg. Chem.* **2009**, *48*, 1577–1587.
- (9) Mirzadeh, N.; Bennett, M. A.; Bhargava, S. K. Cycloaurated complexes of aryl carbanions: Digold(I), digold(II) and beyond. *Coord. Chem. Rev.* **2013**, *257*, 2250–2273.
- (10) Reddy, T. S.; Privér, S. H.; Mirzadeh, N.; Bhargava, S. K. Synthesis of gold(I) phosphine complexes containing the 2-BrC₆F₄PPh₂ ligand: Evaluation of anticancer activity in 2D and 3D spheroidal models of HeLa cancer cells. *Eur. J. Med. Chem.* **2018**, *145*, 291–301.
- (11) Reddy, T. S.; Privér, S. H.; Mirzadeh, N.; Bhargava, S. K. Anticancer gold(I) phosphine complexes: Cyclic trimers and tetramers containing the P-Au-P moiety. *J. Inorg. Biochem.* **2017**, *175*, 1–8.
- (12) Reddy, T. S.; Priver, S. H.; Rao, V. V.; Mirzadeh, N.; Bhargava, S. K. Gold(I) and gold(III) phosphine complexes: Synthesis, anticancer activities towards 2D and 3D cancer models, and apoptosis inducing properties. *Dalton Trans.* **2018**, *47*, 15312–15323.
- (13) Mirzadeh, N.; Privér, S. H.; Abraham, A.; Shukla, R.; Bansal, V.; Bhargava, S. K. Linking flavonoids to gold – A new family of gold compounds for potential therapeutic applications. *Eur. J. Inorg. Chem.* **2015**, *2015*, 4275–4279.
- (14) Mirzadeh, N.; Reddy, T. S.; Bhargava, S. K. Advances in diphosphine ligand-containing gold complexes as anticancer agents. *Coord. Chem. Rev.* **2019**, *388*, 343–359.
- (15) Ganga Reddy, V.; Reddy, T. S.; Privér, S. H.; Bai, Y.; Mishra, S.; Wlodkovic, D.; Mirzadeh, N.; Bhargava, S. Synthesis of gold(I) complexes containing cinnamide: In vitro evaluation of anticancer activity in 2D and 3D spheroidal models of melanoma and in vivo angiogenesis. *Inorg. Chem.* **2019**, *58*, 5988–5999.
- (16) Reddy, T. S.; Pooja, D.; Privér, S. H.; Luwor, R. B.; Mirzadeh, N.; Ramesan, S.; Ramakrishna, S.; Karri, S.; Kuncha, M.; Bhargava, S. K. Potent and selective cytotoxic and anti-inflammatory gold(III) compounds containing cyclometalated phosphine sulfide ligands. *Chem. - Eur. J.* **2019**, *25*, 14089–14100.
- (17) Kilpin, K. J.; Henderson, W.; Nicholson, B. K. Cycloaurated triphenylphosphine-sulfide and -selenide. *Dalton Trans.* **2010**, *39*, 1855–1864.
- (18) Brown, S. D. J.; Henderson, W.; Kilpin, K. J.; Nicholson, B. K. Orthomercurated and cycloaurated derivatives of the iminophosphorane Ph₃PNPh. *Inorg. Chim. Acta* **2007**, *360*, 1310–1315.
- (19) Tabassum, S.; Al-Asbahy, W. M.; Afzal, M.; Arjmand, F. Synthesis, characterization and interaction studies of copper-based drug with Human Serum Albumin (HSA): Spectroscopic and molecular docking investigations. *J. Photochem. Photobiol., B* **2012**, *114*, 132–139.
- (20) Na, N.; Zhao, D. Q.; Li, H.; Jiang, N.; Wen, J. Y.; Liu, H. Y. DNA binding, photonuclease activity and human serum albumin interaction of a water-soluble freebase carboxyl corrole. *Molecules* **2016**, *21*, 54.
- (21) Messori, L.; Abbate, F.; Marcon, G.; Orioli, P.; Fontani, M.; Mini, E.; Mazzei, T.; Carotti, S.; O'Connell, T.; Zanello, P. Gold(III) complexes as potential antitumor agents: Solution chemistry and cytotoxic properties of some selected gold(III) compounds. *J. Med. Chem.* **2000**, *43*, 3541–3548.
- (22) Scheffler, H.; You, Y.; Ott, I. Comparative studies on the cytotoxicity, cellular and nuclear uptake of a series of chloro gold(I) phosphine complexes. *Polyhedron* **2010**, *29*, 66–69.
- (23) Pratesi, A.; Gabbiani, C.; Ginanneschi, M.; Messori, L. Reactions of medicinally relevant gold compounds with the C-terminal motif of thioredoxin reductase elucidated by MS analysis. *Chem. Commun.* **2010**, *46*, 7001–7003.
- (24) Mitsui, A.; Hamuro, J.; Nakamura, H.; Kondo, N.; Hirabayashi, Y.; Ishizaki-Koizumi, S.; Hirakawa, T.; Inoue, T.; Yodoi, J. Overexpression of human thioredoxin in transgenic mice controls oxidative stress and life span. *Antioxid. Redox Signaling* **2002**, *4*, 693–696.
- (25) Zhang, J.; Li, X.; Han, X.; Liu, R.; Fang, J. Targeting the thioredoxin system for cancer therapy. *Trends Pharmacol. Sci.* **2017**, *38*, 794–808.
- (26) Smart, D. K.; Ortiz, K. L.; Mattson, D.; Bradbury, C. M.; Bisht, K. S.; Sieck, L. K.; Brechbiel, M. W.; Gius, D. Thioredoxin reductase as a potential molecular target for anticancer agents that induce oxidative stress. *Cancer Res.* **2004**, *64*, 6716–6724.
- (27) McCall, R.; Miles, M.; Lascuna, P.; Burney, B.; Patel, Z.; Sidoran, K. J.; Sittaramane, V.; Kocerha, J.; Grossie, D. A.; Sessler, J. L.; Arumugam, K.; Arambula, J. F. Dual targeting of the cancer antioxidant network with 1,4-naphthoquinone fused gold(I) N-heterocyclic carbene complexes. *Chem. Sci.* **2017**, *8*, 5918–5929.
- (28) Marzano, C.; Gandin, V.; Folda, A.; Scutari, G.; Bindoli, A.; Rigobello, M. P. Inhibition of thioredoxin reductase by auranofin induces apoptosis in cisplatin-resistant human ovarian cancer cells. *Free Radical Biol. Med.* **2007**, *42*, 872–881.
- (29) Wu, D.; Yotnda, P. Production and detection of reactive oxygen species (ROS) in cancers. *J. Vis. Exp.* **2011**, *57*, e3357.
- (30) van Zijl, F.; Krupitza, G.; Mikulits, W. Initial steps of metastasis: Cell invasion and endothelial transmigration. *Mutat. Res., Rev. Mutat. Res.* **2011**, *728*, 23–34.
- (31) Rodriguez, L. G.; Wu, X.; Guan, J. L. Wound-healing assay. *Cell Migration. Methods in Molecular Biology* **2004**, *294*, 23–29.
- (32) Streicher, K. L.; Sylte, M. J.; Johnson, S. E.; Sordillo, L. M. Thioredoxin reductase regulates angiogenesis by increasing endothelial cell-derived vascular endothelial growth factor. *Nutr. Cancer* **2004**, *50*, 221–231.
- (33) Arnaoutova, I.; Kleinman, H. K. In vitro angiogenesis: Endothelial cell tube formation on gelled basement membrane extract. *Nat. Protoc.* **2010**, *5*, 628–635.
- (34) Namkoong, B.; Güven, S.; Ramesan, S.; Liadanskaya, V.; Abzhanov, A.; Demirci, U. Recapitulating cranial osteogenesis with neural crest cells in 3-D microenvironments. *Acta Biomater.* **2016**, *31*, 301–311.
- (35) Yeo, C. I.; Ooi, K. K.; Tiekink, E. R. T. Gold-based medicine: A paradigm shift in anticancer therapy? *Molecules* **2018**, *23*, 1410.
- (36) Tonelli, M.; Turrell, S.; Cristini-Robbe, O.; El Hamzaoui, H.; Capoen, B.; Bouazaoui, M.; Gazzano, M.; Cassani, M. C. Synthesis of gold nanoparticles within silica monoliths through irradiation techniques using Au(I) and Au(III) precursors. *RSC Adv.* **2014**, *4*, 26038–26045.
- (37) Privér, S. H.; Bennett, M. A.; Willis, A. C.; Pottabathula, S.; Kantam, M. L.; Bhargava, S. K. Ortho-metallated triphenylphosphine chalcogenide complexes of platinum and palladium: Synthesis and catalytic activity. *Dalton Trans.* **2014**, *43*, 12000–12012.
- (38) Uhlén, A.; Åkerström, S. The association of alkali metal N,N-dialkylthiocarbamates in solution. *Acta Chem. Scand.* **1971**, *25*, 393–410.

(39) SMART, ver. 5.625 for the CCD Detector System; Bruker AXS Inc.: Madison, WI, 2001.

(40) SAINTPLUS, ver. 6.22 for the CCD Detector System; Bruker AXS Inc.: Madison, WI, 2001.

(41) Blessing, R. H. An empirical correction for absorption anisotropy. *Acta Crystallogr., Sect. A: Found. Crystallogr.* **1995**, *51*, 33–38.

(42) Sheldrick, G. M. *SHELXTL*, ver. 2013/4; Universität Göttingen: Germany, 2013.

(43) Sheldrick, G. M. A short history of SHELX. *Acta Crystallogr., Sect. A: Found. Crystallogr.* **2008**, *64*, 112–122.